IEEE Access
Multidisciplinary | Rapid Review | Open Access Journal

Received October 23, 2020, accepted November 6, 2020, date of publication November 24, 2020, date of current version December 9, 2020.

Digital Object Identifier 10.1109/ACCESS.2020.3038952

A Cross-Coupled Control Strategy of Phase Difference for Electric Vibration Damping Actuator

ZHENYANG HAO, (Member, IEEE), XUE LI, XIN CAO, (Member, IEEE), YUAN GAN, QIANG YU, AND QIYAO ZHANG, (Student Member, IEEE)
Department of Electrical Engineering, Nanjing University of Aeronautics and Astronautics, Nanjing 210016, China

Corresponding author: Zhenyang Hao (zhenyang_hao@nuaa.edu.cn)

ABSTRACT The active vibration damping actuator uses dual-motors to drive two sets of eccentric wheels to achieve active vibration reduction, but the backlash nonlinearity and eccentric load will cause the load speed and load position to be out of synchronization, which will influence the system vibration reduction effect. The traditional parallel control strategy controls the dual motors separately without the consideration of internal coupling effect, leading to a poor synchronization performance. In order to solve these problems, a load position difference cross-coupled control strategy based on multiple-input and multiple-output (MIMO) is proposed in this paper. The minimum singular value of return difference matrix is used to analyze the stability margin of active vibration damping actuator system under the traditional parallel control strategy and the cross-coupled control strategy, and the analysis procedure has considered the influences of load disturbance and backlash nonlinearity. At the same time, the sensitivity comparison of the two strategies is conducted, and the results indicate that the system under cross-coupled control strategy has stronger relative stability and robustness. On this basis, a method for designing synchronization controller parameters is given. The stability region of parameters satisfying the requirement of stability margin is determined with the help of minimum singular value of return difference matrix. Then, the optimal value is found in the obtained parameter stability region according to the dynamic and steady-state performance. Finally, an experimental platform is set up to verify the effectiveness of cross-coupled control strategy and the rationality of parameter tuning.

INDEX TERMS Electric vibration damping actuator, synchronization, cross-coupled control, stability margin, the minimum singular value, optimal tuning.

I. INTRODUCTION

Helicopters and ships have been increasingly used in military and civil areas, but they experience serious vibrations during operation [1]. Helicopter vibration mainly comes from the load fluctuation caused by the aerodynamic phenomena of the rotor and the blade [2], [3], while the vibration of the ship is the combined effect of propeller, power device and wave [4]. Excessive vibration will not only reduce the driving comfort, but also cause the fatigue of installations. Therefore, reducing the vibration level of helicopters and ships is a task which brooks no delay [5].

Vibration control can be grossly divided into passive type and active type [6]. In recent years, with its advantages of high efficiency and simple structure [7], active vibration control systems have been widely used in helicopters and ships. The principle is to control the actuator to generate the force in the identical amplitude, frequency and the reverse phase to the exciting force according to the vibration signal collected by the vibration sensors [8], [9]. Kenneth D.Garnjost, an American scholar, proposed an electric vibration damping actuator suitable for helicopters in his patent [10]. Applicant discloses that there are two output force modules on each side of the actuator, and each module has a pair of counter-rotating eccentric wheels which are driven by an independent electric servomotor through gears to exert a fixed-amplitude force in the vertical direction. The final force is the superposition of

The associate editor coordinating the review of this manuscript and approving it for publication was Haibin Sun.

the individual forces of the two modules, of which amplitude can be adjusted by changing the position difference between the eccentric wheels on both sides. This invention greatly reduces the weight of the vibration reduction system, and the damping efficiency can reach more than 90%. However, the damping effect largely depends on the strict synchronization of load speed and position difference. The backlash nonlinearity, eccentric load and asymmetric structure all pose great challenges to the synchronous control.

At present, dual-motors synchronous control structures mainly include parallel control, master-slave control, cross-coupled control structure, and so on [11]. Parallel control is realized by giving the same reference signal to each motor in the system, but disturbances applied to one motor will not be reflected on the other motor. The master-slave control divides the two motors into a master motor and a slave motor. The output speed of the master motor is taken as the speed reference for the slave motor, so as to realize the tracking of slave motor to master motor. However, disturbances in the slave motor will not be thrown back to the master. The above two kinds of synchronous control strategies both belong to the decoupled control strategies, which are only applicable to the occasion with no high need for synchronization. In 1980, Koren proposed a dual-motors cross-coupled control strategy [12], which added error feedback on the basis of parallel control strategy, improving the synchronization performance and anti-interference ability. However, the object is to make the position or speed of the two motors identical or maintain a certain ratio, and it cannot adjust the output position difference in real time, which belongs to the single-input single-output (SISO) system. For the electric vibration damping actuator system, it can be regarded as a MIMO system composed of two inputs (position and position difference) and two outputs (positions of two eccentric wheels sets on both side of the actuator). Therefore, the above control strategies are no longer applicable to the electric vibration damping actuator system.

To solve the above problems, a cross-coupled control strategy of load position difference based on MIMO is proposed in this paper. Compared with the traditional parallel control strategy, it improves the speed and position synchronization of loads in the system. The gain margin and phase margin of the system under two control strategies are analyzed and compared by using the minimum singular values of system return difference matrices, and the influences of load disturbance and backlash nonlinearity are considered in the analysis process. In addition, sensitively comparison is conducted with the help of H_∞ control theory. The results demonstrate that the system has a larger stability margin and anti-interference capability under cross-coupled control strategy. Based on that, a parameter tuning method of synchronous controllers is presented. The parameter region, which satisfies the requirements of stability margins, is firstly determined on the basis of the minimum singular value of return difference matrix. Then, the optimization is carried out according to the dynamic and steady-state performance in the stability region. An experimental platform for electric vibration damping actuator system is built, and the experimental results verify the effectiveness of the cross-coupled control strategy and the rationality of parameter tuning.

II. CONTROL STRATEGIES OF ELECTRIC VIBRATION DAMPING ACTUATOR SYSTEM

A. WORKING PRINCIPLE OF ELECTRIC VIBRATION DAMPING ACTUATOR SYSTEM

There are two sets of mechanical parts with identical structure on both sides of the electric vibration damping actuator. The unilateral structure is shown in Fig.1, which is mainly composed of a driving wheel, an idler wheel, two driven wheels and two eccentric wheels. The driven wheel and the eccentric wheel are tightly assembled, and the driving motor is connected to the eccentric wheels through the gear mechanism. The rotation direction of 2# driven wheel is changed through the idler wheel, thereby realizing the reverse rotation of two driven wheels at the same speed.

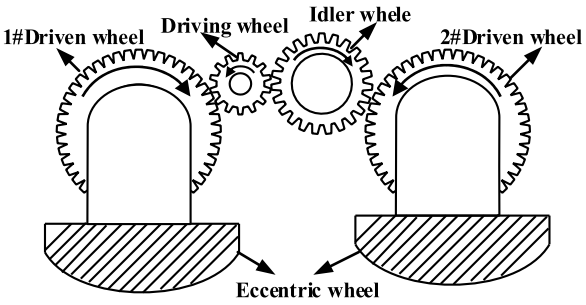

FIGURE 1. Mechanical structure of electric vibration damping actuator.

When analyzing the forces exerted on the eccentric wheels, the eccentric wheels are regarded as particles, as shown in Fig.2. Where m is the mass of the eccentric wheel, ω is its rotational angular velocity, r is the rotational radius, and g is the acceleration of gravity. The angle θ_1 defines the angular position of the eccentric wheel with regard to the vertical axis.

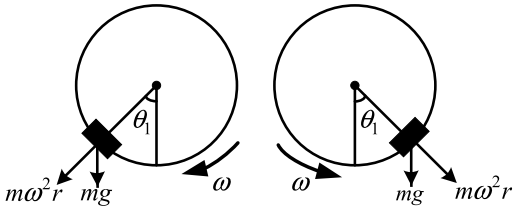

FIGURE 2. Force sketch of eccentric wheels.

When the two eccentric wheels rotate in reverse directions at the same speed, the centrifugal forces cancel each other in the horizontal direction, and superimpose on each other in the vertical direction to balance out the exciting force. The output force generated by the rotating eccentric wheels on one side of the actuator when turning to θ_1 is

$$F_1 = 2m\omega^2 r \cdot \cos\theta_1 \tag{1}$$

Similarly, the output force generated by the eccentric wheels on the other side of the actuator is

$$F_2 = 2m\omega^2 r \cdot \cos\theta_2 \tag{2}$$

The final output force of electric vibration damping actuator is the combination of two individual forces, which can be obtained by adding (1) and (2).

$$F = 4m\omega^2 r \cdot \cos\left(\frac{\theta_1 - \theta_2}{2}\right) \cdot \cos\left(\frac{\theta_1 + \theta_2}{2}\right) \tag{3}$$

where $\theta_1 = \omega t + \psi_1$, $\theta_2 = \omega t + \psi_2$, and ψ is the initial phase of eccentric wheels. Therefore, (3) can be rewritten as

$$F = 4m\omega^2 r \cdot \cos\left(\frac{\theta_1 - \theta_2}{2}\right) \cdot \cos\left(\omega t + \frac{\psi_1 + \psi_2}{2}\right) \tag{4}$$

It is observed that the amplitude and phase controls of the output force are realized by adjusting speed and angular position of the eccentric wheels. Especially, the force amplitude is determined by the position difference between the two sets of eccentric wheels. When the amplitude and frequency of the output force is as same as the exciting force, but opposite in the phase, the object of active vibration reduction can be achieved.

However, it is worth noting that (4) is derived based on the speed synchronization of two sets of eccentric wheels. When the two eccentric wheels sets rotate at different speeds, the final output force will appear beat frequency phenomenon [13], which can not completely offset the exciting force, and the vibration reduction effect will be reduced. Therefore, the control objective of the electric vibration damping actuator system is the strict speed and position difference synchronization of eccentric wheels.

In the electric vibration damping actuator system, due to processing accuracy, it is difficult to guarantee the same technical parameters of each motor and eccentric wheel. The existence of the idler wheel makes 1#driven wheel and 2#driven wheel not completely symmetrical about the motor, which will lead to the speed and position asynchronous. In addition, eccentric load makes larger speed fluctuation. In order to ensure that the gear transmission will not be blocked, the backlash is designed to be large. However, the motor loses the control of the load during the backlash traverse, resulting in the increase of tracking error of the system output. Then, when contact is achieved, the rigid impact of gears will produce impact vibration, leading to performance degradation, and even system instability [14], [15]. All of these above problems impose remarkable limitations on the precision of control. Hence, the traditional parallel control strategy is difficult to meet the requirements of high precision, high robustness and high frequency response of the electric vibration damping actuator system.

B. TRADITIONAL PARALLEL CONTROL STRATEGY

Fig.3 shows the control scheme for vibration damping actuator system based on the traditional parallel independent control strategy, which adopts position, speed and current triple-closed-loops control strategy. Two proportional-integral controllers are implemented in the current loop and speed loop, and the position loop uses pure proportional controller. In Fig.3, APR, ASR and ACR are position regulator, speed regulator and current regulator, respectively.

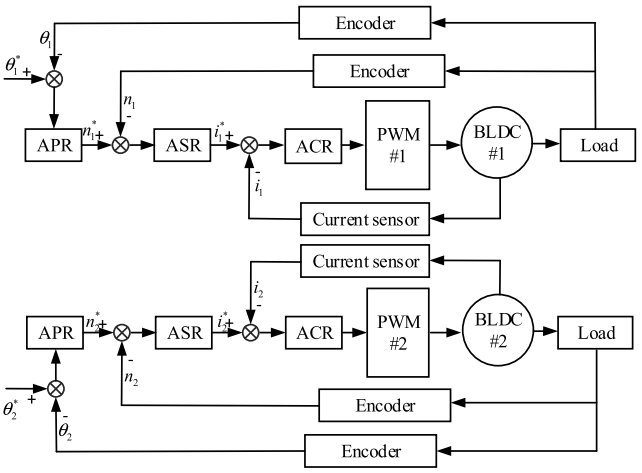

FIGURE 3. Control scheme of vibration damping actuator system based on traditional parallel control strategy.

According to (1)-(4), if the actuator is expected to generate a sinusoidal force with frequency ω^*, initial phase ϕ^*, and amplitude F^*, the given values of the two position loop controllers can be expressed as

$$\begin{cases} \theta_1^* = \omega^* t + \phi^* + \dfrac{\Delta\theta^*}{2} \\ \theta_2^* = \omega^* t + \phi^* - \dfrac{\Delta\theta^*}{2} \end{cases} \tag{5}$$

where

$$\frac{\Delta\theta^*}{2} = \cos^{-1}\left(\frac{F^*}{4m\omega^2 r}\right) \tag{6}$$

The given values are periodic, and the frequency is consistent with the frequency of the output force.

Under the traditional parallel control strategy, the dual motors in the system are independent of each other and disturbances applied to one side of the actuator will not be reflected on the other side. The core of the control is to realize the accurate tracking of the load position in real-time, but the synchronization between two sets of eccentric wheels cannot be guaranteed. Therefore, this control strategy is no longer applicable in high-performance electric vibration damping actuator systems. In this regard, this paper proposes a cross-coupled control strategy of load position difference.

C. CROSS-COUPLED CONTROL STRATEGY

As shown in Fig.4, the control scheme of vibration damping actuator system based on cross-coupled control strategy is mainly composed of four parts: current loop, speed loop, position loop and position difference loop.

The instantaneous position is achieved by averaging the output positions of two sets of eccentric wheels. In this case, the given speed value is calculated by position regulator based on the difference between the instantaneous and given positions. Then, this value is transmitted to dual motors at the same time, so as to realize the speed synchronization.

For the position difference loop, the position difference between two sets of eccentric wheels is multiplied by 1/2 as the feedback value, and then it is sent to the position difference regulator to obtain the relative speed value after making the difference with the given position difference value according to (6). This value is positive for #1 motor and negative for #2 motor. In actual vibration damping actuator system, if the given value is greater than the feedback value, #1 motor accelerates while #2 motor decelerates, thereby rapidly increasing the position difference between the two eccentric wheels sets. When the feedback value is the same as the given value, the position difference loop has no effect on the system, and the dual-motors restore synchronization.

On the basis of the closed-loop controls of the position and position difference, the synchronization of the load speed and the load position difference has been guaranteed. Thereby, the control accuracy of the output force amplitude is improved.

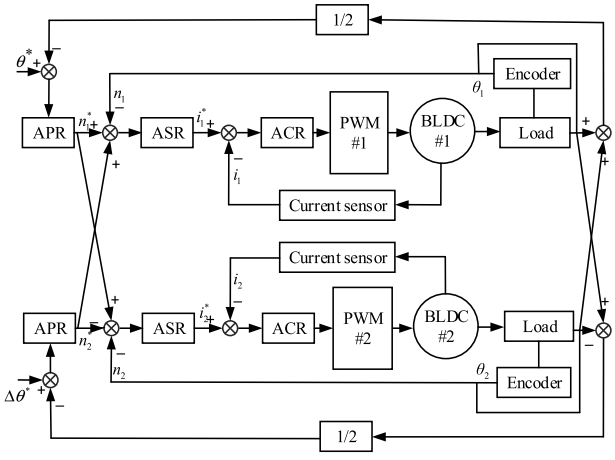

FIGURE 4. Control scheme of vibration damping actuator system based on cross-coupled control strategy.

III. THE STABILITY MARGIN ANALYSIS OF ELECTRIC VIBRATION DAMPING ACTUATOR SYSTEM

A. THE STABILITY MARGIN OF MIMO SYSTEM

The electric vibration damping actuator is a MIMO system. For a multivariable control system, it is no longer applicable to analyze its stability margin by using the Bode diagram or Nyquist curve on the basis of classical control theory. The minimum singular value of the system return difference matrix offers a feasible method to solve this problem [16], [17], which has the advantage of low computation cost.

We can evaluate the stability margin of the system by introducing a disturbance into the original system to make it reach to a critical stable state [18]. The MIMO system utilizes the feedback structure of Fig.5. A measurement matrix $\boldsymbol{L}(s)$ is introduced at the input to examine the gain and phase margins, which is taken as the following diagonal form

$$\boldsymbol{L}(s) = \mathrm{diag}\left\{k_i \exp\left(\mathrm{j}\phi_\mathrm{i}\right)\right\}, \quad \mathrm{i} = 1, 2, 3, \cdots, \mathrm{n} \tag{7}$$

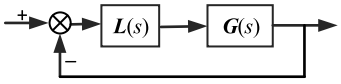

FIGURE 5. Negative feedback control system model.

When the system reaches to the critical stable state, the maximum allowable value of the gain k_i and the phase ϕ_i in all loops are defined as the gain margin and phase margin of the system.

If the system remains stable after introducing the measurement matrix $\boldsymbol{L}(s)$, its return difference matrix should satisfy

$$\underline{\sigma}\left(\boldsymbol{I} + \boldsymbol{LG}\right) > 0 \tag{8}$$

where σ denotes the minimum singular value of the matrix, which is the criteria for measuring system stability margin over the operating frequency. The separation characteristic of the matrix is used to separate $\boldsymbol{L}$ and $\boldsymbol{G}$ from $(\boldsymbol{I} + \boldsymbol{LG})$.

$$\boldsymbol{I} + \boldsymbol{LG} = \left[\left(\boldsymbol{L}^{-1} - \boldsymbol{I}\right)(\boldsymbol{I} + \boldsymbol{G})^{-1} + \boldsymbol{I}\right](\boldsymbol{I} + \boldsymbol{G})\,\boldsymbol{L} \tag{9}$$

Since the electric vibration damping actuator system itself is stable, the return difference matrix $(\boldsymbol{I} + \boldsymbol{G})$ is not singular. Therefore, formula (8) is guaranteed if

$$\overline{\sigma}\left[\left(\boldsymbol{L}^{-1} - \boldsymbol{I}\right)(\boldsymbol{I} + \boldsymbol{G})^{-1}\right] < 1 \tag{10}$$

According to the properties of singular value

$$\bar{\sigma}(\boldsymbol{A})\bar{\sigma}(\boldsymbol{B}) \geq \bar{\sigma}(\boldsymbol{AB}) \tag{11}$$

$$\bar{\sigma}(\boldsymbol{G}) = \frac{1}{\sigma(\boldsymbol{G}^{-1})} \tag{12}$$

where $\bar{\sigma}$ is the maximum singular value of the matrix. The sufficient condition for (10) to be established is

$$\overline{\sigma}\left(\boldsymbol{L}^{-1} - \boldsymbol{I}\right) < \underline{\sigma}\left(\boldsymbol{I} + \boldsymbol{G}\right) \tag{13}$$

Considering that the gain k_i and the phase ϕ_i in each loop of the system change simultaneously, the sufficient condition can be obtained by combining (7), which is equivalent to

$$\bar{\sigma}(\boldsymbol{L}^{-1} - \boldsymbol{I}) = \max_{i=1}^{n} \sqrt{(1 - \frac{1}{k_i})^2 + \frac{2}{k_i}(1 - \cos\phi_i)} \leq \sigma(\boldsymbol{I} + \boldsymbol{G}) \tag{14}$$

Supposing $\bar{\sigma}(\boldsymbol{I} + \boldsymbol{G}) \geq x$, keep the gain $k_i = 1$ and the phase $\phi_i = 0$ respectively in (14), then the gain margin and phase margin in the MIMO system are

$$\mathrm{GM} = -20\lg(1 - x) \quad \mathrm{PM} = \arccos(1 - \frac{x^2}{2}) \tag{15}$$

TABLE 1. The parameters of controllers.

Parameters	K_p	K_i	ω_n rad/s
Current regulator	0.47	768	4560
Speed regulator	1.94	554	796
Position regulator	164.46		161

B. THE STABILITY MARGIN CALCULATION UNDER TWO CONTROL STRATEGIES IN IDEAL CASE

It is assumed that the parameters and structures of the electrical and mechanical components on both sides of the electric vibration damping actuator are identical, and the influences of load fluctuation and backlash nonlinearity are not considered. In order to eliminate the effect of the controller parameters on the relative stability of the system, the cross-coupled system is dispersed into a SISO system for parameter design, and the controller parameters are the same under two control strategies.

When analyzing the position loop, the speed loop can be equivalent to a first-order inertia link since its adjusting process is much faster than that of the position loop. The open-loop transfer function of the position loop is given as

$$G_p(s) = \frac{K_{pp}\omega_n}{s(s+\omega_n)} \tag{16}$$

where K_{pp} is the proportion coefficient of position regulator and ω_n is the open-loop cut-off frequency of speed loop.

The parameters of the motor used in the electric vibration damping actuator are $U_{DC} = 28\text{V}$, $T_{em} = 0.43\text{N}\cdot\text{m}$, $p_n = 7$, $R_m = 0.154\Omega$, and $L_m = 0.094\text{mH}$. According to the method in reference [19], the controller parameters are obtained, as shown in Table I.

The open-loop transfer matrix of the parallel control system is obtained from Fig. 3, which has the following form

$$\boldsymbol{P}_1(s) = \begin{bmatrix} \frac{\theta_1}{\theta_1^*} & \frac{\theta_1}{\theta_2^*} \\ \frac{\theta_2}{\theta_1^*} & \frac{\theta_2}{\theta_2^*} \end{bmatrix} = \begin{bmatrix} \frac{K_{pp}\omega_{cn}}{(s+\omega_{cn})\,s} & 0 \\ 0 & \frac{K_{pp}\omega_{cn}}{(s+\omega_{cn})\,s} \end{bmatrix} \tag{17}$$

The return difference matrix of the system is

$$\boldsymbol{M}_1(s) = \boldsymbol{I} + \boldsymbol{P}_1(s) = \begin{bmatrix} \frac{K_{pp}\omega_{cn}}{(s+\omega_{cn})\,s} + 1 & 0 \\ 0 & \frac{K_{pp}\omega_{cn}}{(s+\omega_{cn})\,s} + 1 \end{bmatrix} \tag{18}$$

According to Fig.4, the open-loop transfer matrix of the system under cross-coupled control strategy is obtained as follows

$$\boldsymbol{P}_2(s) = \begin{bmatrix} \frac{K_{pp}\omega_{cn}}{(s+\omega_{cn})\,s} & \frac{K_{pp}\omega_{cn}}{(s+\omega_{cn})\,s} \\ \frac{K_{pp}\omega_{cn}}{(s+\omega_{cn})\,s} & -\frac{K_{pp}\omega_{cn}}{(s+\omega_{cn})\,s} \end{bmatrix} \tag{19}$$

TABLE 2. Stability margins of control system in the IDEAL CASE.

Control strategy	Minimum singular value	Phase margin	Gain margin
Traditional parallel control	0.88	52.42°	18.67dB
Cross-coupled control	0.85	50.33°	16.50dB

The return difference matrix of the system is

$$\boldsymbol{M_2}(s) = \boldsymbol{I} + \boldsymbol{P_2}(s) = \begin{bmatrix} \frac{K_{pp}\omega_{cn}}{(s+\omega_{cn})\,s} + 1 & \frac{K_{pp}\omega_{cn}}{(s+\omega_{cn})\,s} \\ \frac{K_{pp}\omega_{cn}}{(s+\omega_{cn})\,s} & -\frac{K_{pp}\omega_{cn}}{(s+\omega_{cn})\,s} + 1 \end{bmatrix} \tag{20}$$

The minimum singular values of $\boldsymbol{M}_1(s)$ and $\boldsymbol{M}_2(s)$ are equal to the positive square roots of the minimum eigenvalues of $\boldsymbol{M}_1^{\mathrm{H}}\boldsymbol{M}_1$ and $\boldsymbol{M}_2^{\mathrm{H}}\boldsymbol{M}_2$, respectively, then

$$\underline{\sigma}(\boldsymbol{M}_1) = \min \left| 1 + \frac{K_{pp}\omega_{cn}}{(s+\omega_{cn})\,s} \right|_{\omega\in R^+} \tag{21}$$

$$\underline{\sigma}(\boldsymbol{M}_2) = \min \left| 1 + \sqrt{2}\frac{K_{pp}\omega_{cn}}{(s+\omega_{cn})\,s} \right|_{\omega\in R^+} \tag{22}$$

Substitute the controller parameters in Table I into (21) and (22), and calculate the stability margins according to (15). The results are given in the following Table II.

It can be seen that these two control strategies can keep the electric vibration damping actuator system relatively stable under ideal conditions. However, the load disturbance on the motor will affect the dynamic performance and steady-state accuracy of the system, and the existence of backlash will directly impose an adverse influence on the output quality of the servo system. Therefore, this paper considers the influences of load disturbance and backlash on the system stability margin under two control strategies.

C. THE STABILITY MARGIN CALCULATION UNDER TWO CONTROL STRATEGIES WITH LOAD DISTURBANCE

The load torque of the electric vibration damping actuator is mainly the gravity torque generated by the gravity of eccentric wheels, and its magnitude is determined by the angular position of eccentric wheels, which presents a sinusoidal periodic change. It can be expressed as

$$T_L = \frac{2mgr}{Z}\sin\theta \tag{23}$$

where Z denotes the transmission ratio of the gear set.

The transfer function from the output position of the eccentric wheels to the load disturbance T_L can be described by

$$K(s) = \frac{L_T(T_L)}{L_T(\theta)} = \frac{2mgr}{Z}\frac{s^2}{s^2+\omega^2} \tag{24}$$

It can be proved that the load disturbance is equivalent to a feedback signal introduced into the control system from the output position. The single-sided control block diagram of the actuator system with load disturbance is shown in Fig.6.

TABLE 3. Control system stability margins after introducing load disturbance.

Control strategy	Minimum singular value	Phase margin	Gain margin
Traditional parallel control	0.80	48.35°	14.12dB
Cross-coupled control	0.76	45.57°	12.34dB

Where K_T is the torque constant of the motor, $T_{\sum_n}$ is the time constant of the equivalent first-order inertial link, which is the sum of the time constants of the three-phase inverter bridge and the filter circuit, and J_m is the inertia of motor.

The open-loop transfer function obtained from Fig.6 is

$$\gamma(s) = \frac{APR \cdot ASR \cdot K_T}{J_m s^2 (T_{\sum n} s + 1) + K(s)(T_{\sum n} s + 1) + ASR \cdot K_T s} \tag{25}$$

Therefore, the return difference matrices under two control strategies can be easily derived

$$\boldsymbol{M}_1'(s) = \begin{bmatrix} \gamma(s)+1 & 0 \\ 0 & \gamma(s)+1 \end{bmatrix} \tag{26}$$

$$\boldsymbol{M}_2'(s) = \begin{bmatrix} \gamma(s)+1 & \gamma(s) \\ \gamma(s) & -\gamma(s)+1 \end{bmatrix} \tag{27}$$

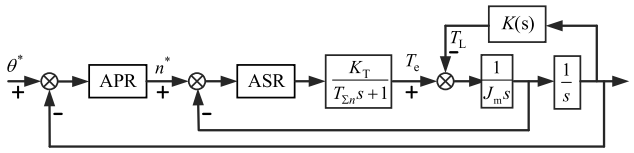

FIGURE 6. Single-sided control block diagram of vibration damping actuator system with load disturbance.

The minimum singular values of system return difference matrices are given by

$$\underline{\sigma}(\boldsymbol{M}_1') = \min |1 + \gamma(s)|_{\omega \in R^+} \tag{28}$$

$$\underline{\sigma}(\boldsymbol{M}_2') = \min \left| 1 + \sqrt{2}\gamma(s) \right|_{\omega \in R^+} \tag{29}$$

Substitute the specific motor and controller parameters into (28) and (29), and calculate the corresponding stability margin according to (15). The results are shown in Table III.

It can be seen that after the introduction of sinusoidal load disturbance, the stability margins under these two strategies are still close, and there is no significant change compared with the ideal case, indicating that these two control strategies both have anti-interference capability. Therefore, when analyzing the stability margin of the system with backlash, ignore the influence of load disturbance so as to facilitate the analysis.

D. THE STABILITY MARGIN CALCULATION UNDER TWO CONTROL STRATEGIES WITH BACKLASH

According to Fig.1, multiple backlashes are used to connect the motor and eccentric wheels, which affect system performance and even cause instability. Therefore, it is necessary to select appropriate control strategy to weaken the adverse effect of backlash on system stability. The two eccentric wheels on one side of the actuator are converted to the driving wheel to 1# driven wheel side, so that the backlash only acts between the driving wheel and 1# driven wheel. The output torque T_o described by the dead-zone model can be expressed as [20]

$$T_o = \begin{cases} k\,[z-\alpha] & z > \alpha \\ 0 & |z| \le \alpha \\ k\,[z+\alpha] & z < -\alpha \end{cases} \tag{30}$$

where k is the stiffness coefficient, z is the relative displacement between the driving wheel and driven wheel and α is half of the backlash gap size. The transfer function of the dead-zone model is obtained by using descriptive function technique [21]

$$N(A) = \frac{2k}{\pi}\left(\frac{\pi}{2} - arc\sin\frac{\alpha}{A} - \frac{\alpha}{A}\sqrt{1-\frac{\alpha^2}{A^2}}\right) \quad A \ge \alpha \tag{31}$$

where A is the amplitude of angle difference between the driving wheel and driven wheel.

Therefore, the control block diagram of one side of the electric vibration damping actuator with backlash is established as shown in Fig.7.

According to Fig.7, we can get

$$Q(s) = \frac{APR \cdot ASR \cdot K_n}{J_1 s^2 + ASR \cdot K_n s + P(s)} \tag{32}$$

Where $P(s)$ and K_n can be calculated as

$$P(s) = \frac{2 \cdot N(A) \cdot s^2}{s^2 + \frac{N(A)}{J_2}} \tag{33}$$

$$K_n = \frac{K_T}{T_{\Sigma n} s + 1} \tag{34}$$

It is difficult to guarantee the same backlash size on both sides of the actuator due to the machining error. As a result, the open-loop transfer functions on both sides are different.

$$Q_1(s) \ne Q_2(s) \tag{35}$$

The return difference matrices of the system under two control strategies are given by the following expression

$$\boldsymbol{M}_1''(s) = \begin{bmatrix} Q_1(s)+1 & 0 \\ 0 & Q_2(s)+1 \end{bmatrix} \tag{36}$$

$$\boldsymbol{M}_2''(s) = \begin{bmatrix} Q_1(s)+1 & Q_1(s) \\ Q_2(s) & -Q_2(s)+1 \end{bmatrix} \tag{37}$$

It is obvious from (31) that the backlash is mainly related to the amplitude of angle difference and the backlash size. Suppose $A_1 = 0.5$mm, $\alpha_1 = 0.1$mm, change the values of A_2 and α_2 to explore the influence of backlash on system stability margin. The results are shown in Fig.8. It can be seen that the minimum singular value of system return difference matrix under parallel control strategy is greatly reduced after the introduction of backlash, with maximum decline of 67.22%. While the stability margin of the system under

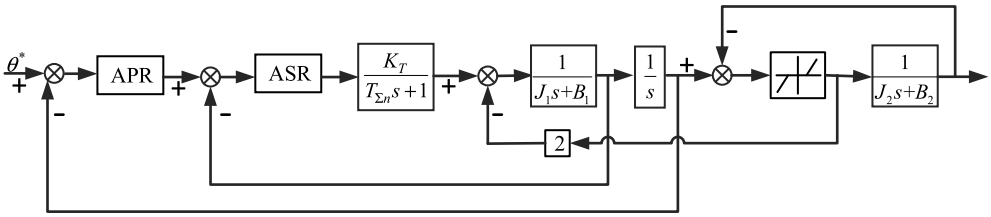

FIGURE 7. Single-sided control block diagram of vibration damping actuator system with backlash.

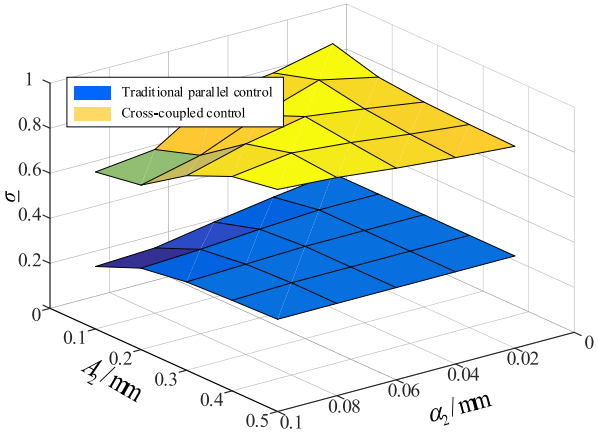

FIGURE 8. Comparison chart of minimum singular values with two different control strategies.

cross-coupled control strategy only drops by 14.53%, which means cross-coupled control strategy can weaken the adverse effect of backlash on system stability margin and ensure the dynamic performance and steady-state accuracy of the final output force.

IV. THE SENSITIVITY ANALYSIS OF ELECTRIC VIBRATION DAMPING ACTUATOR SYSTEM

In the actual flight process, the helicopter will bring different types of external random disturbances to the actuator. Therefore, it is expected that the vibration damping actuator system not only has good stability margins, but also owns good robustness. According to the characteristics of helicopter operation conditions, a random load position disturbance υ is introduced into the position loop and system sensitivity is analyzed by H_∞ control theory [22], [23].

If $\boldsymbol{T}(s)$ is the transfer function matrix from the disturbance to the control error, then its H_∞ norm is defined as [24]:

$$\|\boldsymbol{T}\|_\infty = \sup_\omega \overline{\sigma}\{\boldsymbol{T}(j\omega)\} \tag{38}$$

where sup is the supremum.

According to the concept of operate norm, the norm of $\boldsymbol{T}$ is defined as:

$$\|\boldsymbol{T}\| = \sup_{\upsilon\neq 0} \frac{\|\boldsymbol{T}\upsilon\|_2}{\|\upsilon\|_2} \tag{39}$$

Therefore, when $\boldsymbol{T} \in H_\infty$ and $\upsilon \in L_2(-\infty, \infty)$, we can draw the following conclusion

$$\|\boldsymbol{T}\| = \sup_{\upsilon\neq 0} \frac{\|\boldsymbol{T}\upsilon\|_2}{\|\upsilon\|_2} = \sup_\omega \overline{\sigma}\{\boldsymbol{T}(j\omega)\} = \|\boldsymbol{T}\|_\infty \tag{40}$$

Formula (38) shows that the H_∞ norm is the induced norm of the system 2-norm in H_∞ space, indicating that the H_∞ norm represents the maximum gain of the signal from the disturbance to the control error. Consequently, it can be concluded that the smaller the H_∞ norm of system transfer function is, the lower the influence of external disturbance υ on the control error of the system.

The sensitivity stability margin is defined as $||\boldsymbol{T}(s)||^{-1}$, which is a supplement to the gain margin and phase margin [18].

The closed-loop transfer function matrices from disturbance to control error under two control strategies are given by

$$\boldsymbol{T}_1(s) = \begin{bmatrix} \dfrac{s+\omega_n}{s^2+\omega_n s+K_{pp}\omega_n} \\ 0 \end{bmatrix} \tag{41}$$

$$\boldsymbol{T}_1(s) = \begin{bmatrix} \dfrac{s+\omega_n}{2s^2+2\omega_n s+2K_{pp}\omega_n} \\ \dfrac{s+\omega_n}{2s^2+2\omega_n s+2K_{pp}\omega_n} \end{bmatrix} \tag{42}$$

The respective H_∞ norms of $\boldsymbol{T}_1$ and $\boldsymbol{T}_2$ are calculated in MATLAB as 0.01 and 0.0071, hence the sensitivity stability margins of systems under two control strategies are 100 and 140.8, respectively, indicating that the cross-coupled control strategy has an improved control performance in robustness.

V. PARAMETER TUNING OF SYNCHRONOUS CONTROLLERS OF ELECTRIC VIBRATION DAMPING ACTUATOR

A. PARAMETER TUNING OF SYNCHRONOUS CONTROLLERS BASED ON STABILITY MARGINS

From the comparisons in the above section, it can be seen that after considering the load disturbance and backlash nonlinearity, the cross-coupled control strategy still keeps the system stability margin in a relatively good range. However, its controllers are designed by dispersing the system into a SISO system, indicating that the parameters are often not optimal. For this reason, considering the coupling effect, this paper presents an optimal tuning method for the parameters of

synchronization regulators of the electric vibration damping actuator system, which is based on the stability margins. The speed loop and current loop both belong to the inner loops of the motor and can be designed by the method in reference [16].

According to the analyses in Section III C, D, it is obvious that the cross-coupled control strategy can weaken the influences of backlash nonlinearity and sinusoidal load disturbance on the stability margins. Therefore, when designing the parameters of synchronization controllers, these influences can be ignored. Both the position loop and the position difference loop adopt pure proportional regulators, and the proportional coefficients are both K_{pp}. It is assumed that the gain margin and phase margin of the system should be 6.3dB $\leq$ GM $\leq$ 20dB and 45° $\leq$ PM $\leq$ 70° respectively, the minimum singular value range of the return difference matrix is set to (0.7653, 0.9) according to (15).

By inserting $s = j\omega$, the minimum singular value of the system return difference matrix under the cross-coupled control strategy is

$$\underline{\sigma}(j\omega) = \left|1 + \sqrt{2}\frac{GH}{j\omega}\right| = \left|\frac{\sqrt{2}K_{pp}\omega_{cn}}{j\omega(j\omega + \omega_{cn})} + 1\right| \tag{43}$$

Squaring (43), then there is

$$\underline{\sigma}^2(j\omega) = \frac{\left(\sqrt{2}K_{pp}\omega_{cn} - \omega^2\right)^2 + (\omega_{cn}\omega)^2}{\omega^4 + (\omega_{cn}\omega)^2}, \quad \omega \in (0, +\infty) \tag{44}$$

Taking the derivative of (44), the minimum value of $\square\sigma^2(j\omega)$ in the system operating frequency range is given by

$$\underline{\sigma}^2(j\omega)_{\min} = \frac{-2K_{pp}\omega_{cn}}{\sqrt{K_{pp}^2\omega_{cn}^2 + \sqrt{2}K_{pp}\omega_{cn}^3} + K_{pp}\omega_{cn} + \frac{\sqrt{2}}{2}\omega_{cn}^2} + 1 \tag{45}$$

Thus, the relationship between the minimum singular value of system return difference matrix and the proportional coefficient of synchronous controllers is established. After sorting out (45), we have the following expression

$$(1 - t^2)K_{pp}^2\omega_{cn}^2 + (\sqrt{2}\omega_{cn}^2 - \sqrt{2}t\omega_{cn}^2)K_{pp}\omega_{cn} = \frac{\omega_{cn}^4}{2} \tag{46}$$

where $t = [\underline{\sigma}(j\omega)^2 + 1]/[\underline{\sigma}(j\omega)^2 - 1]$. The proportional coefficient of synchronization controllers can be expressed as

$$\begin{cases} K_{PP} = \omega_{cn}\dfrac{\sqrt{2}(t-1) - 2\sqrt{1-t}}{2(1-t^2)} \\ t = \dfrac{\underline{\sigma}^2(j\omega) + 1}{\underline{\sigma}^2(j\omega) - 1}, 0.7653 \leq \underline{\sigma}(j\omega) \leq 0.9 \end{cases} \tag{47}$$

Consequently, the range of proportional coefficient of synchronous controllers satisfying the requirements of stability margins under cross-coupled control strategy is (94.8,327.2).

B. PARAMETER OPTIMIZATION

When designing the parameters of the synchronization controllers, it is necessary to seek optimal control parameters in the obtained stability region, so as to give consideration to the dynamic and steady-state performance. The specific method is to find the characteristic roots of the system characteristic equation according to the state coefficient matrix, and then draw the step response curve of the system with the characteristic roots. The step responses under different parameters are shown in Fig.9. It can be observed that with the increase of K_{pp}, the dynamic settling time is shortened, but the overshoot and static error will increase at the same time, which will cause the output position of the actuator deviate and affect the vibration reduction performance. Therefore, the proportional coefficient is determined as 150 in consideration of dynamic characteristic and steady-state accuracy. At this time, the dynamic settling time is less than 0.05s with no static error and overshoot.

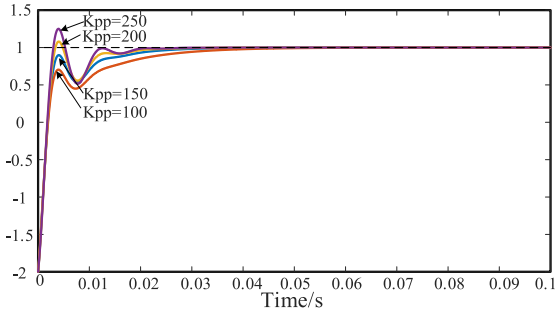

FIGURE 9. System step response curve under different K_{pp}.

VI. EXPERIMENTAL VERIFICATION

In order to verify the achievable of the parameter design and to investigate the effectiveness of the cross-coupled control strategy, experiments are carried out on a platform of vibration damping system shown in Fig.10. The output force is collected by the force sensor, and an absolute magnetic encoder has been applied to achieve accurate measurements of load speed and load position. The performance of the cross-coupled control strategy proposed in this paper is compared with the tradition parallel control strategy.

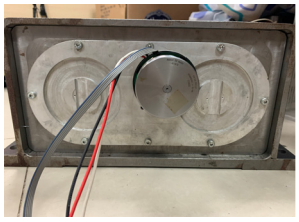

FIGURE 10. The prototype of electric vibration damping actuator.

Table IV lists the performance indices of the electric vibration damping actuator.

TABLE 4. The performance indices of ELECTRIC vibration damping actuator.

Description	Parameters
Rated operating frequency /Hz	21.5
working band /Hz	19~23
Minimum output force /N	≤100
Settling time of frequency change 1Hz /s	≤0.5
Frequency error	≤0.1%
Settling time of amplitude change 300N /s	≤0.5
Steady-state error of force amplitude	≤5%
Settling time of phase change 180°/s	≤0.5
Steady-state error of phase	≤5%

A. EXPERIMENTAL COMPARISON AND VERIFICATION OF SYNCHRONISM BETWEEN LOAD SPEED AND POSITION DIFFERENCE

The reference phase difference is πrad, at which time the output force of the electric vibration damping actuator is theoretically 0. Fig.11 are waveforms of load speed difference, load position difference and minimum output force under parallel control strategy and cross-coupled control strategy.

From Fig.11(a), it can be seen that the speed difference between dual motors on both sides of the actuator under cross-coupled control strategy ranges from -40rpm to 40rpm, which is only 1/4 of that under parallel control strategy. Fig.11(b) shows that the cross-coupled control has smoother position difference and faster convergence speed compared with the tradition parallel control strategy. The position difference errors of these two strategies are less than 0.02rad and 0.11rad, respectively. It can be seen from Fig.11(c) that the amplitude of the minimum output force under cross-coupled control strategy is reduced by 1/2 compared with that under the traditional parallel control strategy, which meets the index requirement of the minimum output force less than 100N. Fig.11 indicates that under cross-coupled control strategy, better synchronizations of load speed and position are achieved such that a better control accuracy of output force is obtained.

B. EXPERIMENTAL COMPATISON AND VERIFICATION OF ACTUATOR OUTPUT FORCE PERFORMANCE

When the flag bit signal is high, sequentially send commands of amplitude increase of 300N, frequency increase of 1Hz and phase change of 180°. Comparative experimental results are shown in Fig.12, 13 and 14.

As can be seen in Fig.12, the output force under cross-coupled control strategy has smaller overshoot and dynamic settling time than that under parallel control strategy when the force amplitude is stepped up by 300N. From Fig.13, it can be seen that compared with the dynamic settling time of 0.7s when the output force changes from 21.5Hz to 22.5Hz under parallel control strategy, the output force can quickly converge to the corresponding reference frequency within 0.32s under cross-coupled control strategy. In Fig.14, the performance is examined under the phase step change. When the

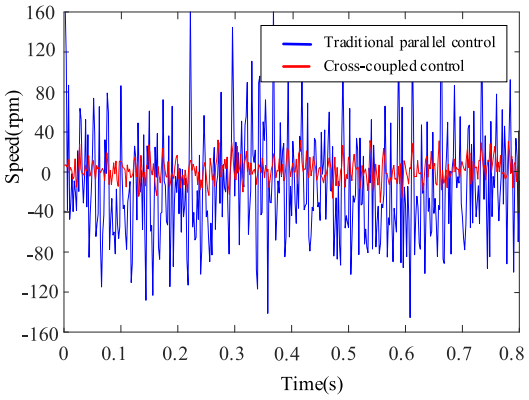

(a) Speed difference

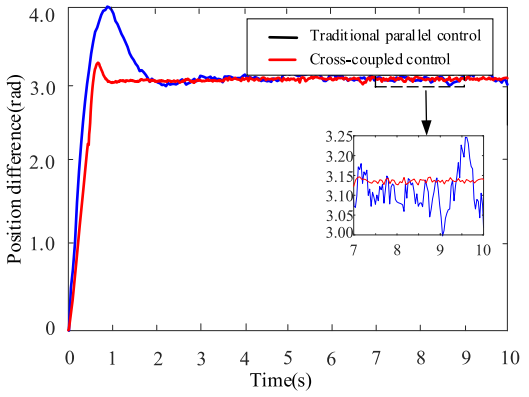

(b) Load position difference

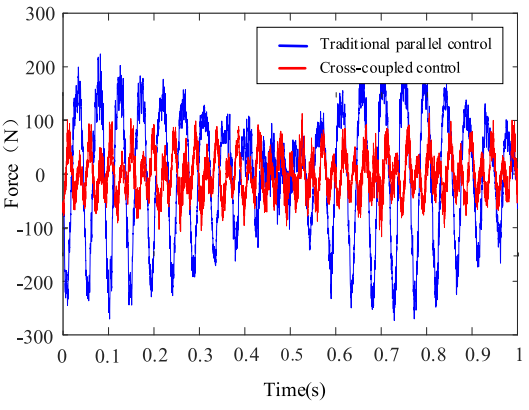

(c) Minimum output force of actuator

FIGURE 11. Speed difference, load position difference and minimum output force of the electric vibration damping actuator under two control strategies.

parallel control strategy is adopted, the settling time for the output force phase changing 180° is 0.9s, and the steady-state error is 60°. When the system adopts the cross-coupled control strategy, the dynamic settling time is only 0.48s with no steady-state error.

According to above experimental results, it can be proved that a better dynamic tracking performance is obtained with the help of the cross-coupled control strategy, indicating the excellent performance of the cross-coupled control

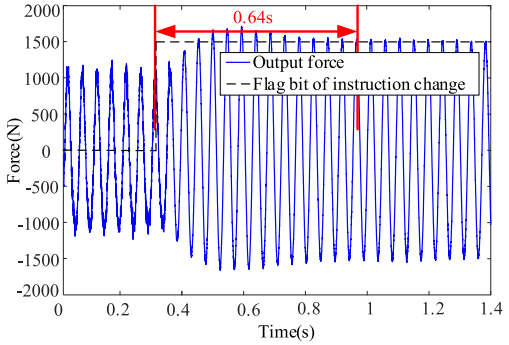

(a)Traditional parallel control.

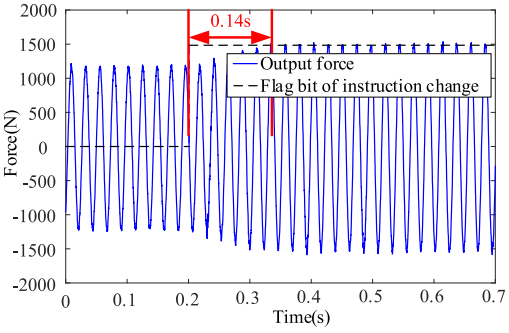

(b)Cross-coupled control.

FIGURE 12. Waveforms of output force with amplitude change of 300N under two control strategies.

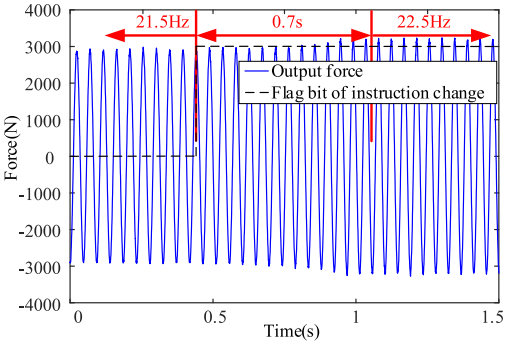

(a)Traditional parallel control.

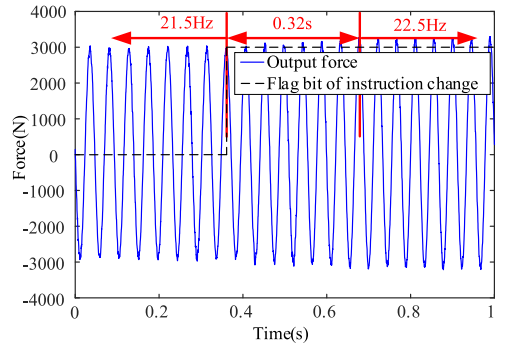

(b)Cross-coupled control.

FIGURE 13. Waveforms of output force with frequency change of 1Hz under two control strategies.

strategy and the rationality of the parameter tuning method in Section V.

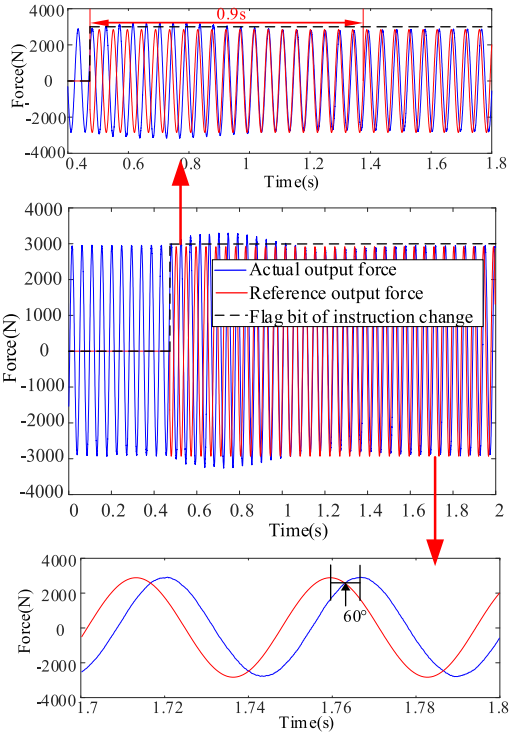

(a)Traditional parallel control.

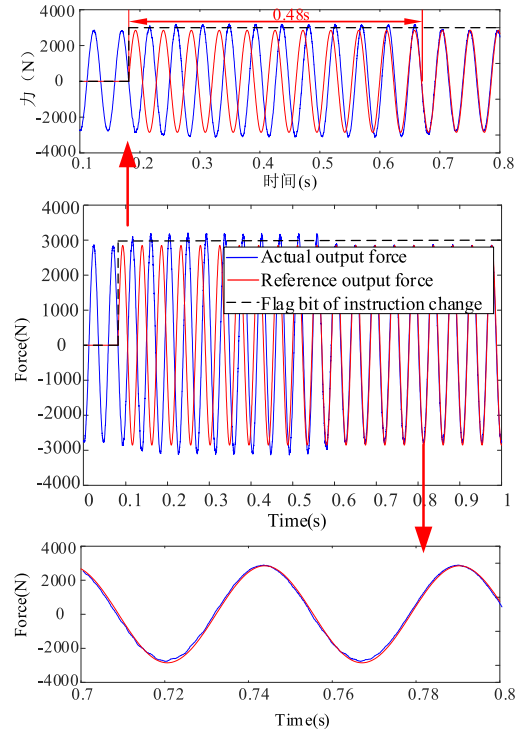

(b)Cross-coupled control.

FIGURE 14. Waveforms of output force with 180° phase change under two control strategies.

VII. CONCLUSION

In this paper, a cross-coupled control strategy based on load position difference is proposed to solve the problems of speed and position non-synchronization caused by eccentric load

and backlash nonlinearity in the vibration damping actuator. The following conclusions are obtained:

a. In the cross-coupled control strategy, the input position value of the cross-coupled control strategy obtains the speed reference value through the function of the position loop, and the dual motors track the reference signal to realize the synchronization of speed. Meanwhile, on the basis of the closed-loop control of the position difference between the eccentric wheels sets on both sides of the actuator, the synchronization of the load position difference has been achieved. Comparative experimental results verified the effectiveness and superiority of the cross-coupled control strategy in synchronization performance.

b. The stability margins of the vibration damping actuator system are analyzed by the minimum singular value of return difference matrix, and the system sensitivity is analyzed by H_∞ control theory. Comparative results indicate that the cross-coupled control strategy can maintain the stability margin of the system in a relatively good range after considering backlash and possess stronger robustness for stochastic disturbance. Thereby, the dynamic and steady-state performance of the final output force has significantly improved.

c. A systematic procedure on the synchronization controllers parameters design is given in this paper. The stability region of the control parameters, which satisfies the requirements of stability margins, is firstly determined on the basis of the minimum singular value of system return difference matrix. Then, in the resultant stability region, the optimal parameter is obtained by comparing and analyzing the distribution of eigenvalues under the state coefficient matrix. Experimental results verify the rationality of the parameter design.

REFERENCES

[1] J. Y. Wang, Y. Y. Song, and C. L. Shen, "Modern helicopter cockpit system and its prospects," *Aeronaut. Manuf. Technol.*, no. 9, pp. 38–40, Oct. 2006.

[2] P. P. Friedmann, "Rotary-wing aeroelasticity: Current status and future trends," *AIAA J.*, vol. 42, no. 10, pp. 1953–1972, 2004.

[3] M. V. Lowson, "Progress towards quieter civil helicopters," *Aeronaut. J. New Ser.*, vol. 96, no. 956, pp. 209–223, Jun. 1992.

[4] J. Guo, G. Li, B. Li, and S. Wang, "A ship active vibration isolation system based on a novel 5-DOF parallel mechanism," in *Proc. IEEE Int. Conf. Inf. Autom. (ICIA)*, Hailar, China, Jul. 2014, pp. 800–805.

[5] R. Ganguli, "Optimum design of a helicopter rotor for low vibration using aeroelastic analysis and response surface methods," *J. Sound Vib.*, vol. 258, no. 2, pp. 327–344, Nov. 2002.

[6] P. Gardonio and S. J. Elliott, "Passive and active isolation of structural vibration transmission between two plates connected by a set of mounts," *J. Sound Vib.*, vol. 237, no. 3, pp. 483–511, Oct. 2000.

[7] W. L. Liu, Z. T. Mu, and C. M. Duan, "Research on vibration and vibration reduction characteristic of helicopter," *J. Nav. Aeronaut. Eng. Inst.*, vol. 19, no. 5, pp. 533–536, Jul. 2004.

[8] C. Qi-You, D. Jing-Hui, H. Jian-Ping, L. Ai-Min, and L. Ke, "Optimization selection approach for distribution of actuators in active vibration control of helicopter," in *Proc. 34th Chin. Control Conf. (CCC)*, Hangzhou, China, Jul. 2015, pp. 3248–3251.

[9] D.-H. Kim, T.-J. Kim, S.-K. Paek, D.-I. Kwak, and S.-U. Jung, "Application and performance evaluation of helicopter active vibration control system for surion," *J. Korean Soc. Aeronaut. Space Sci.*, vol. 43, no. 6, pp. 557–567, Jun. 2015.

[10] K. D. Garnjost and J. G. Rey, "Modular vibratory force generator, and method of operating same," U.S. Patant 5 903 077, May 11, 1999.

[11] Y. B. Wang and K. Cao, "Brief introduction of multi-motor synchronous control technology," *Small Special Electr. Mach.*, vol. 47, no. 08, pp. 69–73, Aug. 2019.

[12] Y. Koren, "Cross-coupled biaxial computer control for manufacturing systems," *J. Dyn. Syst., Meas., Control*, vol. 102, no. 4, pp. 265–275, Dec. 1980.

[13] P. Vartholomeos, K. Vlachos, and E. Papadopoulos, "Analysis and motion control of a centrifugal-force microrobotic platform," *IEEE Trans. Autom. Sci. Eng.*, vol. 10, no. 3, pp. 545–553, Jul. 2013.

[14] Y. L. Ma, J. Huang, and D. Zhang, "Adaptive compensation of backlash nonlinearity for servo systems," *J. Syst. Simul.*, vol. 21, no. 5, pp. 1498–1501 and 1504, May 2009.

[15] A. Lagerberg and B. Egardt, "Backlash estimation with application to automotive powertrains," *IEEE Trans. Control Syst. Technol.*, vol. 15, no. 3, pp. 483–493, Jun. 2007.

[16] V. Mukhopadhyay and J. Newsom, "Application of matrix singular value properties for evaluating gain and phase margins of multiloop systems," in *Proc. AIAA Guid. Navigat. Control Conf.*, Sacramento, CA, USA, 1982, pp. 420–428.

[17] Q.-G. Wang, Y. He, Z. Ye, C. Lin, and C. C. Hang, "On loop phase margins of multivariable control systems," *J. Process Control*, vol. 18, no. 2, pp. 202–211, Feb. 2008.

[18] F. C. Zhai, Z. K. Shi, and G. Z. Dai, "Several definitions of MIMO system stability margin," *Flight Dyn.*, vol. 20, no. 2, pp. 6–9, Jun. 2002.

[19] Z. M. Han, "Research on control strategy of PMSM direct drive position servo system," M.S. thesis, Nanjing Univ. Aeronaut. Astronaut., Nanjing, China, 2017.

[20] Z. Shi and Z. Zuo, "Backstepping control for gear transmission servo systems with backlash nonlinearity," *IEEE Trans. Autom. Sci. Eng.*, vol. 12, no. 2, pp. 752–757, Apr. 2015.

[21] J. O. Jang, P. G. Lee, H. T. Chung, and G. J. Jeon, "Output backlash compensation of systems using fuzzy logic," in *Proc. Amer. Control Conf.*, Denver, CO, USA, 2003, pp. 2489–2490.

[22] W. Che and G. Yang, "Non-fragile state feedback H-infinity control for discrete-time systems with quantized signals," *J. Control Theory Appl.*, vol. 7, no. 1, pp. 63–67, Feb. 2009.

[23] B. Q. Xi, Y. Li, H. Xia, Q. Li, and C. Wang, "H2/H_∞ controller design in attitude control system of aerocraft," in *Proc. Int. Conf. Mechatronics Autom.*, Changchun, China, 2009, pp. 577–581.

[24] T. Kitamoto and T. Yamaguchi, "Parametric computation of H_∞ norm of a system," in *Proc. SICE-ICASE Int. Joint Conf.*, Busan, South Korea, 2006, pp. 3181–3184.

ZHENYANG HAO (Member, IEEE) received the bachelor's degree in electrical engineering from Nanjing Normal University, in 2004, and the master's and Ph.D. degrees in power electronics and motion drive from the Nanjing University of Aeronautics and Astronautics, in 2010.

He has been an Associate Professor with the Department of Electrical Engineering, Nanjing University of Aeronautics and Astronautics, since 2013. His research interests include new energy power electronic conversion technology, aviation power supply and power actuator technology, and electric vehicle motor design and driving technology.

XUE LI graduated in electrical engineering from the Nanjing University of Aeronautics and Astronautics, China, in 2018, where she is currently pursuing the master's degree in electrical engineering.

Her current research interest includes multi-motor coordinated control.

XIN CAO (Member, IEEE) received the B.Eng., M.Sc., and Ph.D. degrees in electrical engineering from the Nanjing University of Aeronautics and Astronautics, Nanjing, China, in 2003, 2006, and 2010, respectively, all in electrical engineering.

From June 2011 to September 2012, he was a Research Associate with the Department of Aeronautical and Automotive Engineering, Loughborough University, Loughborough, U.K. Since 2011, he has been with the Nanjing University of Aeronautics and Astronautics. His current research interests include distributed generation and renewable energy, electric vehicles, switched reluctance motors, and magnetically levitated bearingless motors.

YUAN GAN received the B.Eng. degree in electrical engineering from the Anhui University of Science and Technology, Hefei, in 2017, and the M.Sc. degree in electrical engineering from the Nanjing University of Aeronautics and Astronautics, Nanjing, China, in 2020. His current research interest includes servo motor control.

QIANG YU received the B.Eng. degree in electrical engineering from the Jiangsu University of Science and Technology, Zhenjiang, in 2017, and the M.Sc. degree in electrical engineering from the Nanjing University of Aeronautics and Astronautics, Nanjing, China, in 2020. His current research interest includes bearingless switched reluctance motors.

QIYAO ZHANG (Student Member, IEEE) graduated in electrical engineering and automation from the Nanjing University of Aeronautics and Astronautics, China, in 2020, where she is currently pursuing the master's degree in electrical engineering. Her current research interest includes motor control.